# Supporting information

## Rational Design of Efficient Orange-Red to Red Thermally Activated Delayed Fluorescence Emitters for OLEDs with External Quantum Efficiency up to 26.0% and Reduced Efficiency Roll-off

Jixiong Liang, Chenglong Li,* Yuanyuan Cui, Zhiqiang Li, Jiaxuan Wang, and Yue Wang*

State Key Laboratory of Supramolecular Structure and Materials, College of Chemistry, Jilin University, Changchun 130012, P. R. China

## Table of Contents

1. **General Information**
2. **Single Crystal X-Ray Crystallography and X-ray data of PXZ-PQM**
3. **Theoretical Calculations**
4. **Device Fabrication and Measurement**
5. **Calculation Formulas**
6. **Figures S1-S9**
7. **Tables S1-S2**
8. **Spectra data**
9. **References**

## 1. General Information

$^1$H NMR spectra were measured on Varian Mercury 500 MHz spectrometer. Mass spectrum was recorded on a GC/MS mass spectrometer. Elemental analyses were performed on a flash EA 1112 spectrometer. UV-vis absorption spectra were recorded by a Shimadzu UV-2550 spectrophotometer. The emission spectra were recorded by a Shimadzu RF-5301 PC spectrometer. The absolute fluorescence quantum yields of doped films were measured on Edinburgh FLS920 steady state fluorimeter. Thermogravimetric analyses (TGA) were carried out on a TA Q500 thermogravimeter by measuring their weight loss while heating at a rate of 10 °C min$^{-1}$ from 25 to 800 °C under nitrogen. Differential scanning calorimetric (DSC) measurements were performed on a NETZSCH DSC204 instrument at a heating rate of 10 °C min$^{-1}$ from 20 to 450 °C under a nitrogen atmosphere. Electrochemical measurements were performed with a BAS 100W Bioanalytical electrochemical work station, using Pt as working electrode, platinum wire as auxiliary electrode, and a porous glass wick Ag/Ag$^+$ as pseudo-reference electrode, standardized against ferrocene/ferrocenium. The oxidation and reduction potentials of **PXZ-PQM**, **DPXZ-PQM** and **DPXZ-DPPM** were measured in $CH_2Cl_2$ and DMF solution containing 0.1 M of *n*-$Bu_4NPF_6$ as a supporting electrolyte at a scan rate of 100 mV s$^{-1}$.

## 2. Single Crystal X-Ray Crystallography

Diffraction data were collected on a Rigaku RAXIS-PRID diffractometer using the ω-scan mode with graphite-monochromator Mo•Kα radiation. The structure was solved with direct methods using the SHELXTL programs and refined with fullmatrix least-squares on $F^2$. Non-hydrogen atoms were refined anisotropically. The positions of hydrogen atoms were calculated and refined isotropically. The corresponding CCDC reference number (CCDC: 1943981) and the

data can be obtained free of charge from The Cambridge Crystallographic Data Centre via www.ccdc.cam.ac.uk/data_request/cif.

## 3. Theoretical Calculations

The ground state geometries were fully optimized by the density functional theory (DFT).[S1] The lowest singlet excited state ($S_1$) and the lowest triplet excited state ($T_1$) were calculated by time-dependent DFT (TDDFT).[S2] All the above calculations were carried out at the B3LYP/6-31G (d) level by using the Gaussian 16, Revision A.03 software package.[S3]

## 4. Device Fabrication and Measurement

TAPC, TCTA, DCzDPy and B3PymPm were purchased from Xi'an Polymer Light Technology Corp. Before device fabrication, the ITO glass substrates were pre-cleaned carefully and treated by oxygen plasma for 3 min. Then the sample was transferred to the deposition system. The devices were prepared in vacuum at a pressure of $5 \times 10^{-4}$ Pa. The organic materials were thermally evaporated at a rate of 1.0 Å $s^{-1}$. After the organic film deposition, 1 nm of LiF and 100 nm of aluminum were thermally evaporated onto the organic surface. The thicknesses of the organic materials and the cathode layers were controlled using a quartz crystal thickness monitor. The electrical characteristics of the devices were measured with a Keithley 2400 source meter. The EL spectra and luminance of the devices were obtained on a PR655 spectrometer. All the devices fabrication and device characterization steps were carried out at room temperature under ambient laboratory conditions.

## 5. Calculation Formulas

The calculation formulas for the rate constants of fluorescent ($k_F$), internal conversion ($k_{IC}$), inter-system crossing ($k_{ISC}$), TADF ($k_{TADF}$) and reverse intersystem crossing ($k_{RISC}$) are expressed as following list:[S4]

$$k_F = \Phi_F/\tau_F \quad \text{(S1)}$$

$$\Phi = k_F/(k_F + k_{IC}) \quad \text{(S2)}$$

$$\Phi_F = k_F/(k_F + k_{IC} + k_{ISC}) \quad \text{(S3)}$$

$$\Phi_{ISC} = k_{ISC}/(k_F + k_{IC} + k_{ISC}) \quad \text{(S4)}$$

$$k_{TADF} = \Phi_{TADF}/(\Phi_{ISC}\ \tau_{TADF}) \quad \text{(S5)}$$

$$k_{RISC} = k_F\ k_{TADF}\ \Phi_{TADF}/(k_{ISC}\ \Phi_F) \quad \text{(S6)}$$

## 6. Figures

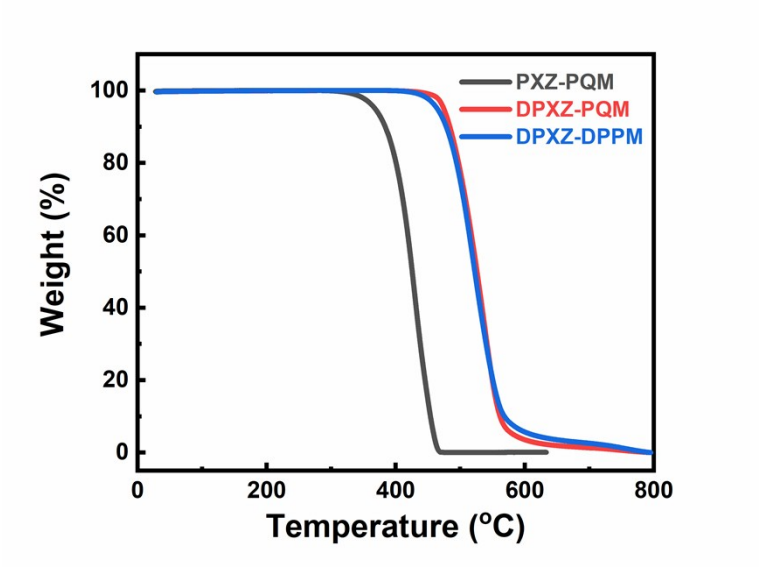


**Fig. S1** Thermal gravimetric analysis (TGA) of **PXZ-PQM**, **DPXZ-PQM** and **DPXZ-DPPM**.

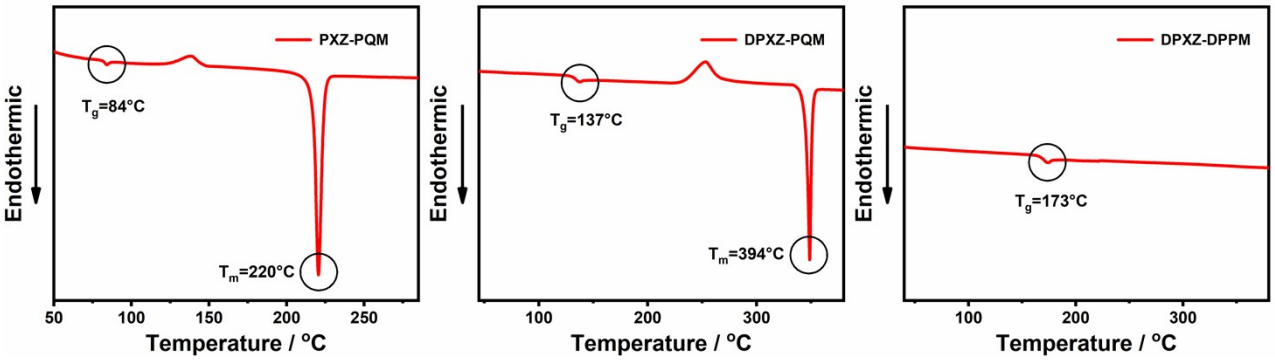


**Fig. S2** Differential scanning calorimetry (DSC) of **PXZ-PQM**, **DPXZ-PQM** and **DPXZ-DPPM**.

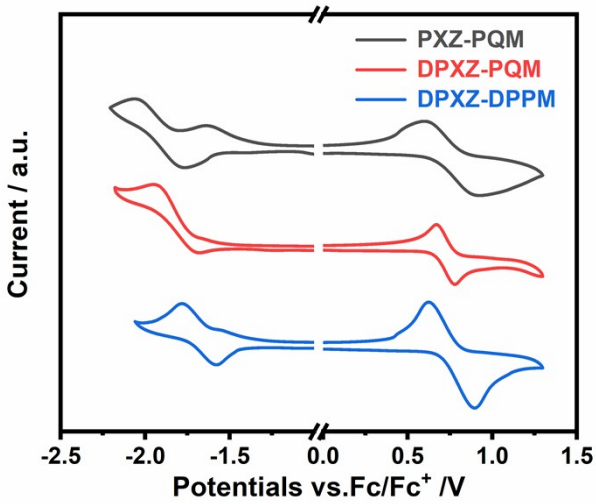


**Fig. S3** Oxidization and reduction potentials of **PXZ-PQM**, **DPXZ-PQM** and **DPXZ-DPPM**. The oxidation and reduction potentials were measured in DCM and DMF solutions, respectively.

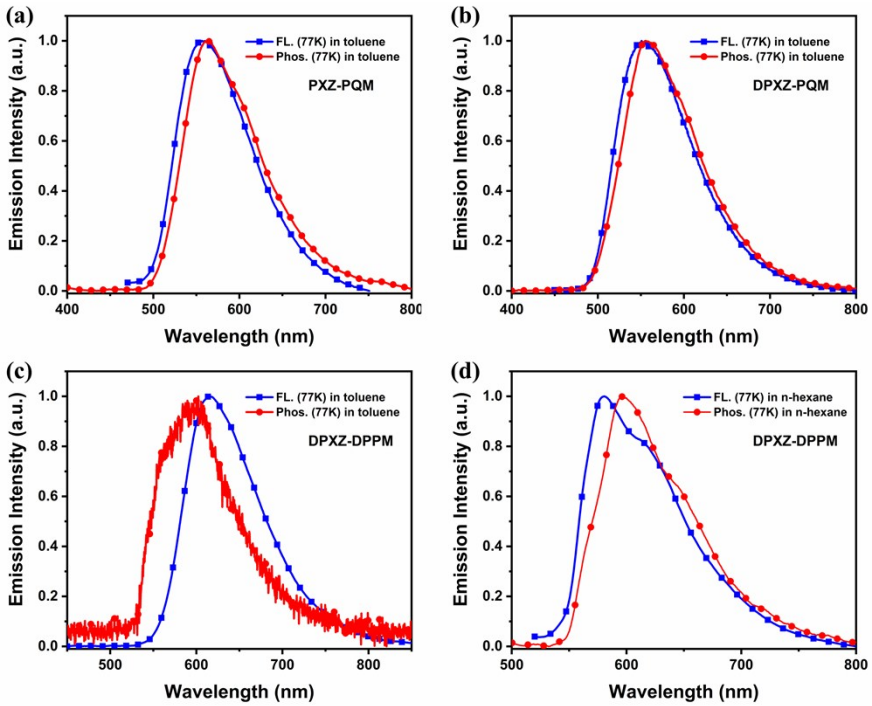


**Fig. S4** Fluorescence (FL.) and phosphorescence (Phos.) spectra of **PXZ-PQM** (a), **DPXZ-PQM** (b) and **DPXZ-DPPM** (c) in toluene ($10^{-5}$ M) at 77 K, and FL. and Phos. spectra of **DPXZ-DPPM** (d) in n-hexane ($10^{-5}$ M) at 77 K.

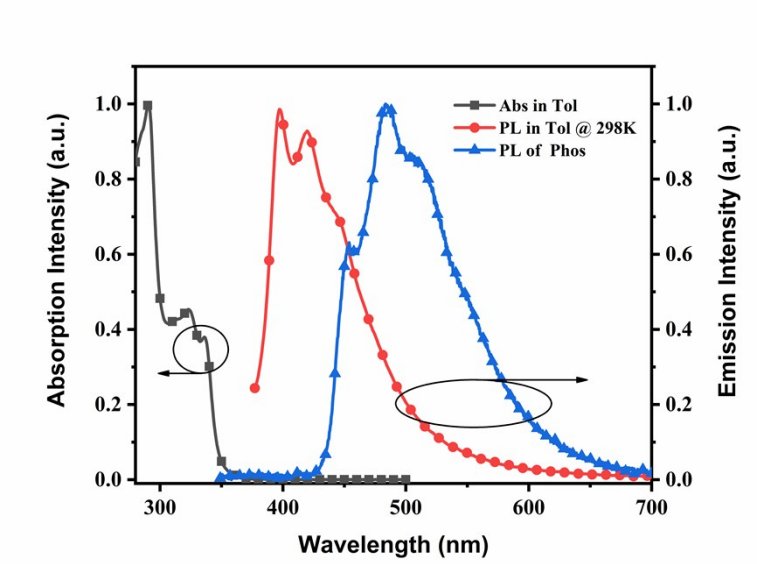


**Fig. S5** The absorption, fluorescence (298 K) and phosphorescence (77 K) spectra of DCzDPy in toluene ($10^{-5}$ M).

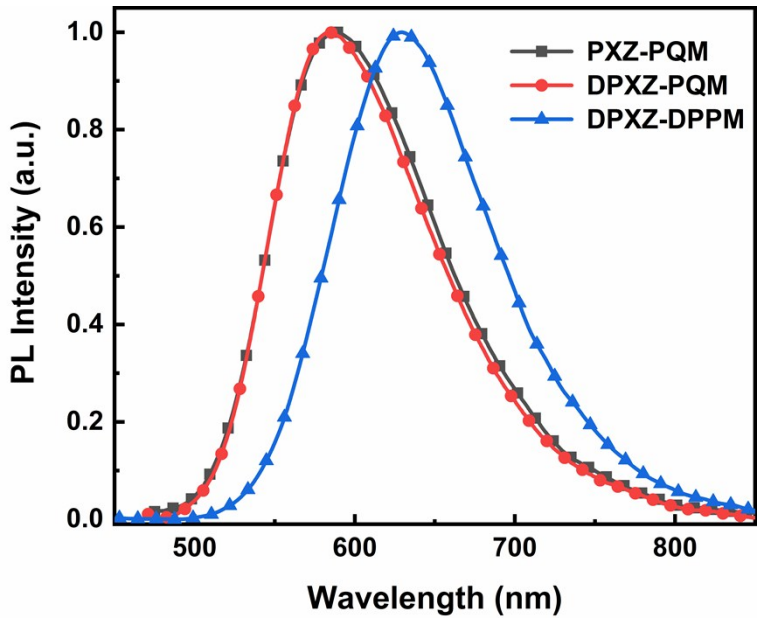


**Fig. S6** The PL spectra of **PXZ-PQM**, **DPXZ-PQM** and **DPXZ-DPPM** 5% doped DCzDPy film at room temperature.

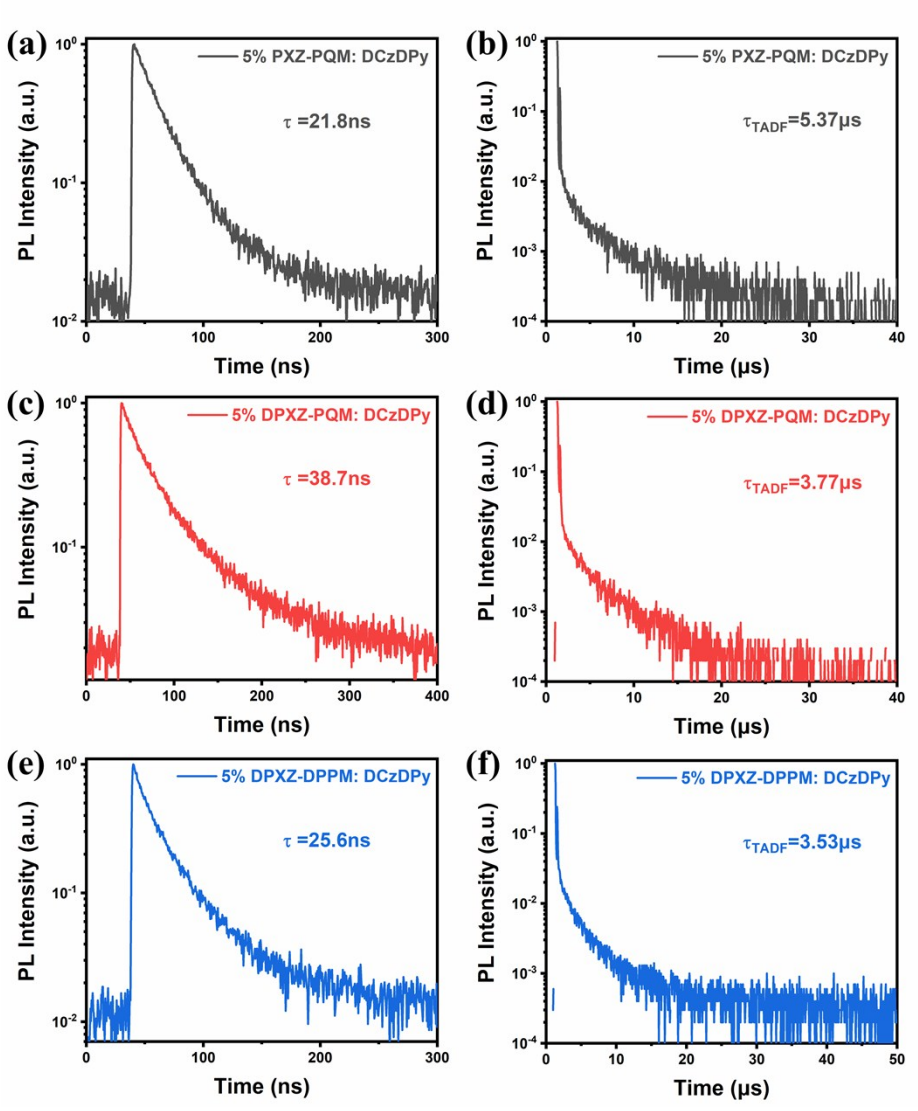


**Fig. S7** The room temperature transient decay curves of **PXZ-PQM** (a, b), **DPXZ-PQM** (c, d) and **DPXZ-DPPM** (e, f) 5% doped DCzDPy film.

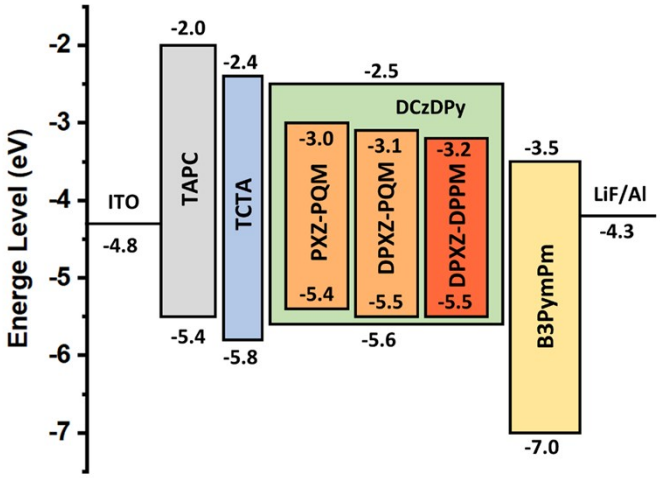


**Fig. S8** The device structure and energy level diagram and molecular structures of the materials employed in the devices.

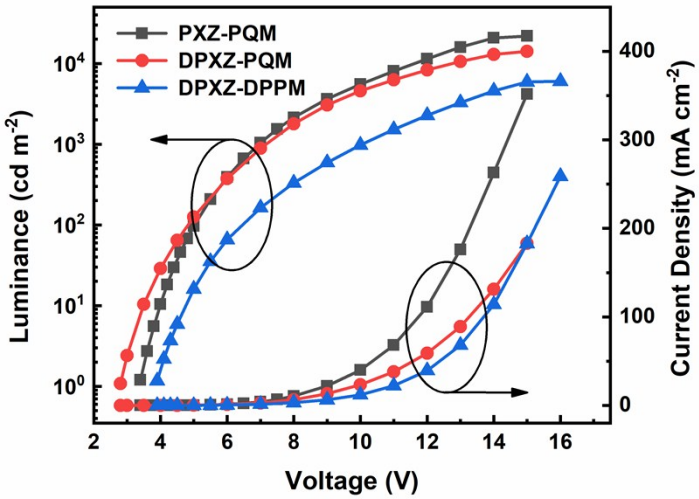


**Fig. S9** Current density−voltage−brightness (*J*−*V*−*L*) characteristics of **PXZ-PQM**, **DPXZ-PQM**, and **DPXZ-DPPM** based devices

## 7. Tables

**Table S1** Crystal data and structure refinement for **PXZ-PQM**.

| | | |
|---|---|---|
| Identification code | PXZ-PQM | |
| Empirical formula | C33 H21 N3 O2 | |
| Formula weight | 491.53 | |
| Temperature | 100(2) K | |
| Wavelength | 0.71073 Å | |
| Crystal system | Monoclinic | |
| Space group | $P2_1/c$ | |
| Unit cell dimensions | a = 20.1020(15) Å | a= 90°. |
| | b = 13.4448(10) Å | b= 98.084(3)° |
| | c = 8.9583(6) Å | g = 90° |
| Volume | 2397.1(3) $Å^3$ | |
| Z | 4 | |
| Density (calculated) | 1.362 $Mg/m^3$ | |
| Absorption coefficient | 0.086 $mm^{-1}$ | |
| F(000) | 1024 | |
| Crystal size | 0.300 x 0.300 x 0.005 $mm^3$ | |
| Theta range for data collection | 2.821 to 25.998°. | |
| Index ranges | -24<=h<=24, -16<=k<=16, -11<=l<=11 | |
| Reflections collected | 59642 | |
| Independent reflections | 4697 [R(int) = 0.0496] | |
| Completeness to theta = 25.242° | 99.9 % | |
| Absorption correction | None | |
| Refinement method | Full-matrix least-squares on $F^2$ | |
| Data / restraints / parameters | 4697 / 585 / 343 | |
| Goodness-of-fit on $F^2$ | 1.007 | |
| Final R indices [I>2sigma(I)] | R1 = 0.0406, wR2 = 0.1203 | |
| R indices (all data) | R1 = 0.0524, wR2 = 0.1297 | |
| Extinction coefficient | n/a | |
| Largest diff. peak and hole | 0.268 and -0.215 $e.Å^{-3}$ | |

**Table S2** The transient PL delay data of 5% PXZ-PQM, DPXZ-PQM, and DPXZ-DPPM doped films at different temperature.

| Compound | $\tau_d$ [μs]$^{a)}$/$R_d^{b)}$ | | |
|---|---|---|---|
| | 100 K | 200 K | 300 K |
| **PXZ-PQM** | 0.91/7.46% | 1.00/10.79% | 2.06/31.95% |
| **DPXZ-PQM** | 0.64/19.11% | 0.98/21.71% | 2.06/31.05% |
| **DPXZ-DPPM** | 3.19/50.12% | 3.06/62.89% | 2.56/63.69% |

[a] PL lifetimes of delayed fluorescence ($\tau_d$). [b] The weighting factors for delayed fluorescence.

**Table S3** Summarized transient PL data and rate constants of PXZ-PQM, DPXZ-PQM, and DPXZ-DPPM.

| Emitter[a] | PLQY [%][b] | $\Phi_{PL}$ [%][c] | $\Phi_{TADF}$ [%][d] | $\tau_p$ [ns][e] | $\tau_d$ [μs][f] | $k_F$ [$10^7$ $s^{-1}$][g] | $k_{IC}$ [$10^7$ $s^{-1}$][h] | $k_{ISC}$ [$10^7$ $s^{-1}$][i] | $k_{TADF}$ [$10^5$ $s^{-1}$][j] | $k_{RISC}$ [$10^5$ $s^{-1}$][k] | $\Phi_{ISC}$ [%][l] |
|---|---|---|---|---|---|---|---|---|---|---|---|
| PXZ-PQM | 70 | 53.5 | 16.6 | 21.8 | 5.4 | 2.45 | 1.05 | 1.08 | 1.30 | 0.91 | 23.64 |
| DPXZ-PQM | 88 | 60.6 | 27.4 | 38.7 | 3.8 | 1.57 | 0.21 | 0.81 | 2.33 | 2.05 | 31.16 |
| DPXZ-DPPM | 61 | 38.1 | 22.9 | 25.6 | 3.5 | 1.49 | 0.95 | 1.47 | 1.73 | 1.05 | 37.52 |

[a] 5% emitters doped in DCzDPy film (100 nm) at 298 K. [b] The total fluorescence quantum yield. [c] The prompt fluorescent component of PLQY. [d] The delayed fluorescent component of PLQY. [e] The lifetimes of prompt fluorescent. [f] The lifetimes of TADF. [g] The rate constants of fluorescent. [h] The rate constants of internal conversion. [i] The rate constants of intersystem crossing. [j] The rate constants of TADF. [k] The rate constants of reverse intersystem crossing. [l] The efficiency of ISC.

8. Spectra data:

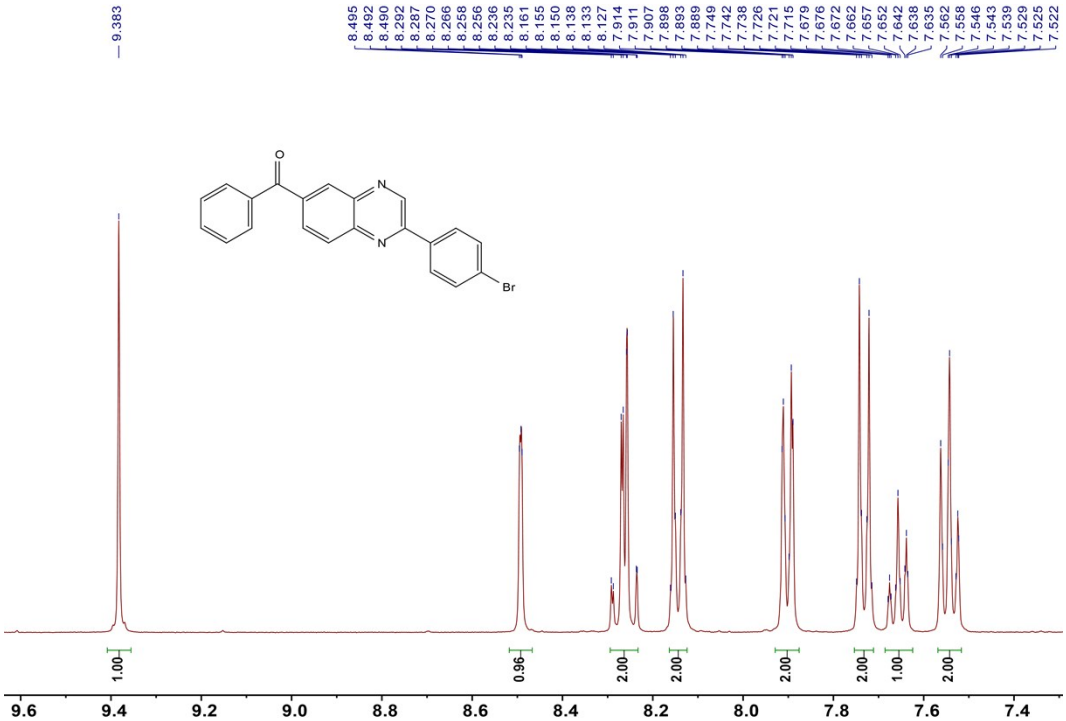


Fig. S8 $^{1}$H NMR spectrum of **Br-PQM** in $CDCl_3$.

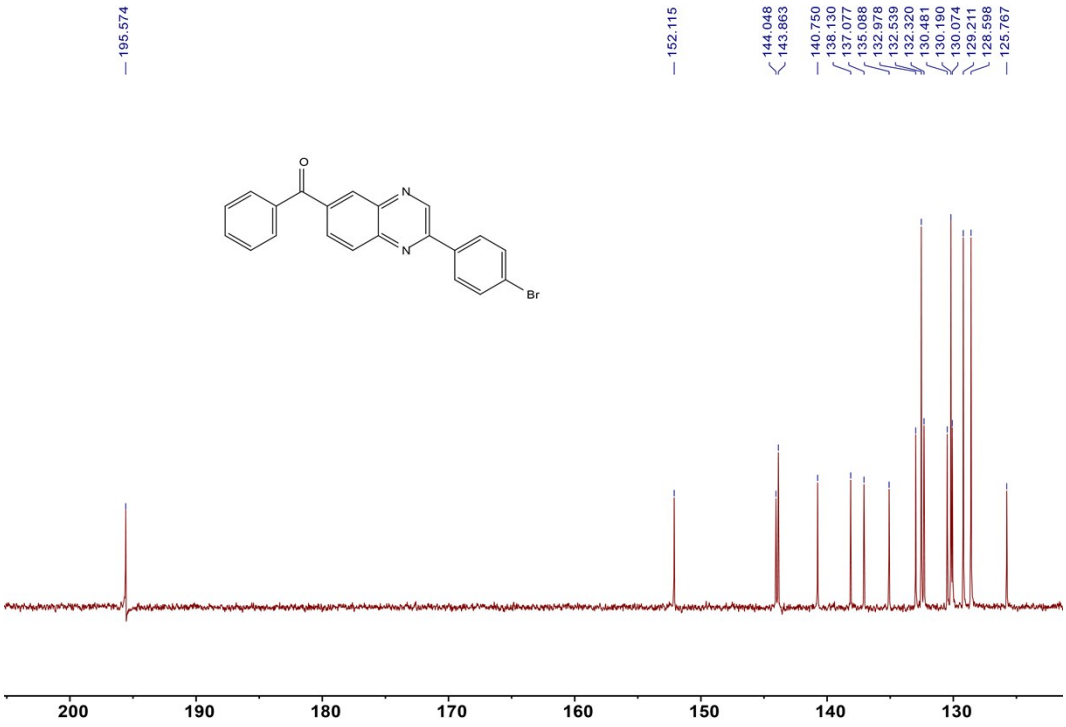

Fig. S9 $^{13}C$ NMR spectrum of **Br-PQM** in $CDCl_3$.

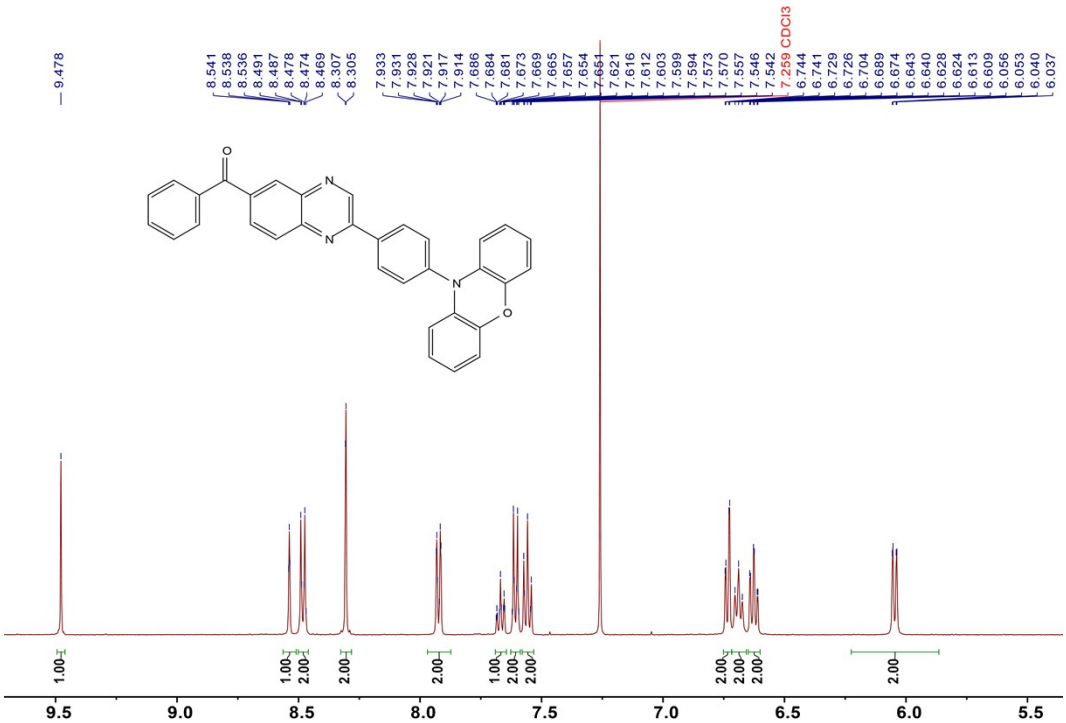


Fig. S10 $^{1}H$ NMR spectrum of **PXZ-PQM** in $CDCl_3$.

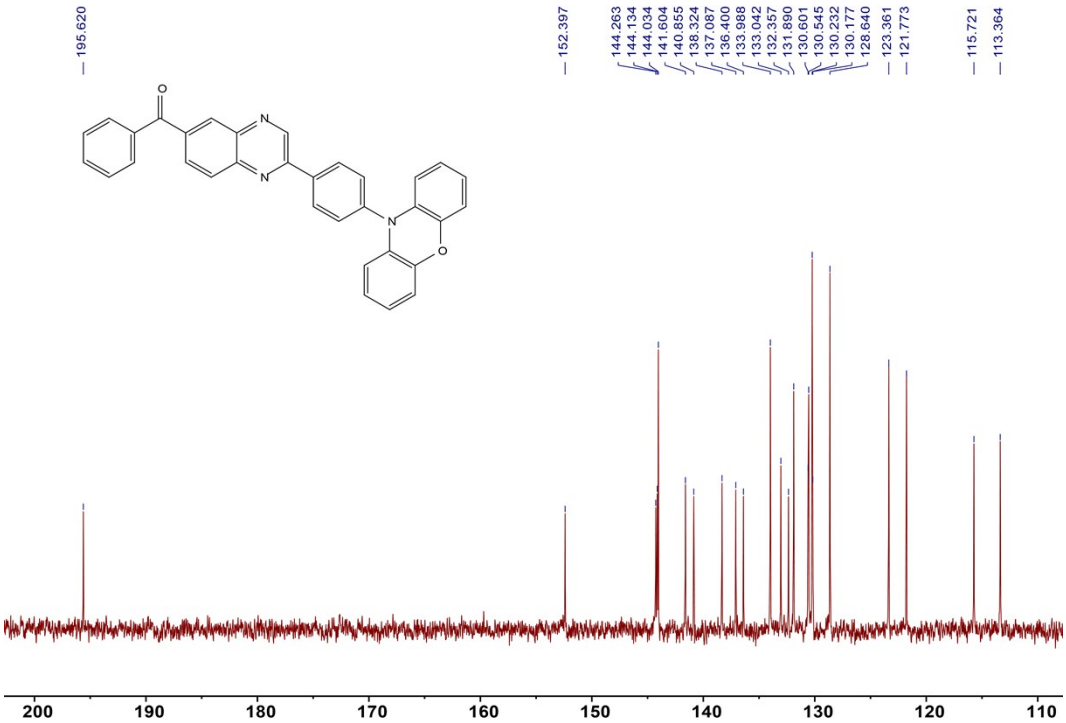

Fig. S11 $^{13}C$ NMR spectrum of **PXZ-PQM** in $CDCl_3$.

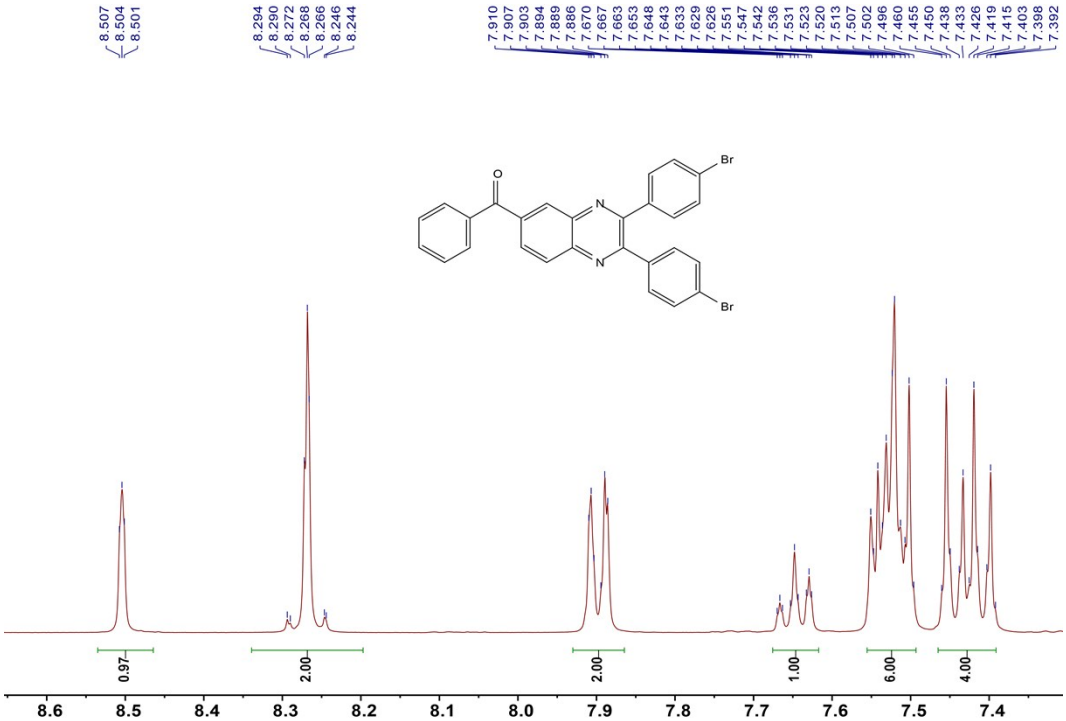


Fig. S12 $^{1}H$ NMR spectrum of **DBr-PQM** in $CDCl_3$.

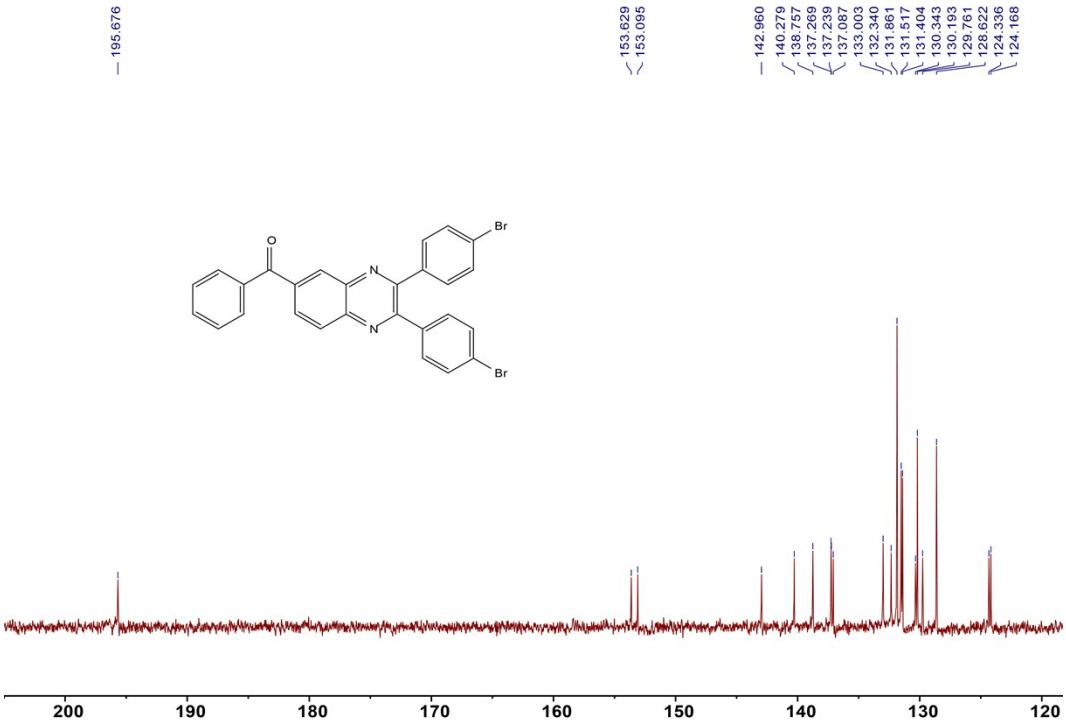

Fig. S13 $^{13}C$ NMR spectrum of **DBr-PQM** in $CDCl_3$.

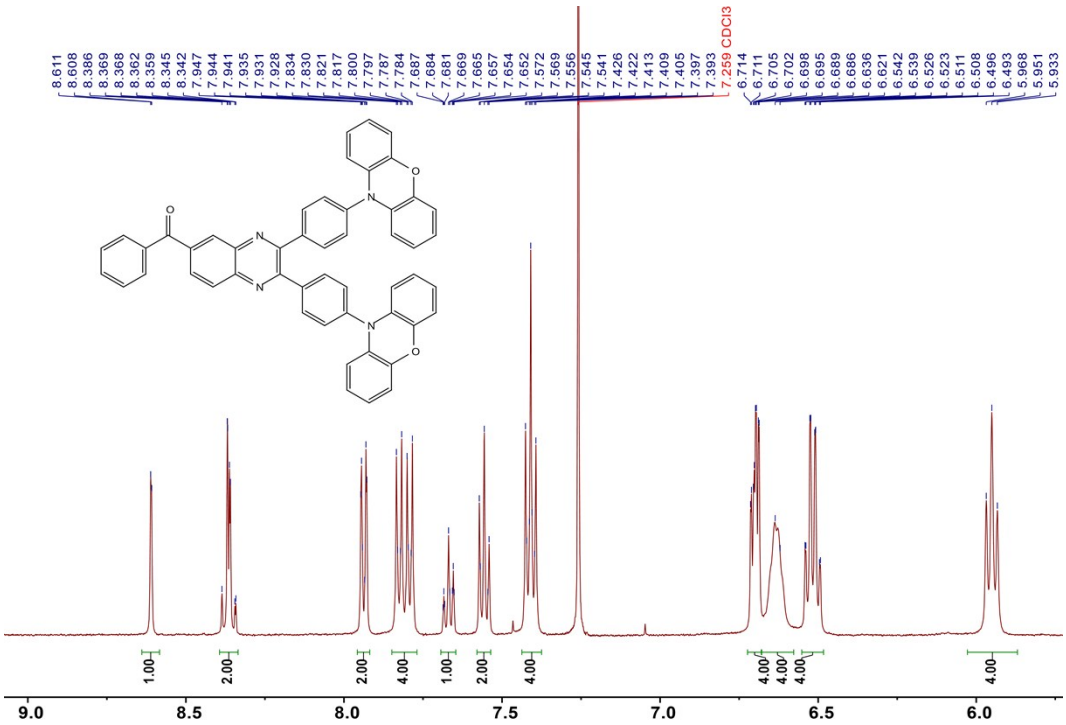


Fig. S14 $^{1}H$ NMR spectrum of **DPXZ-PQM** in $CDCl_3$.

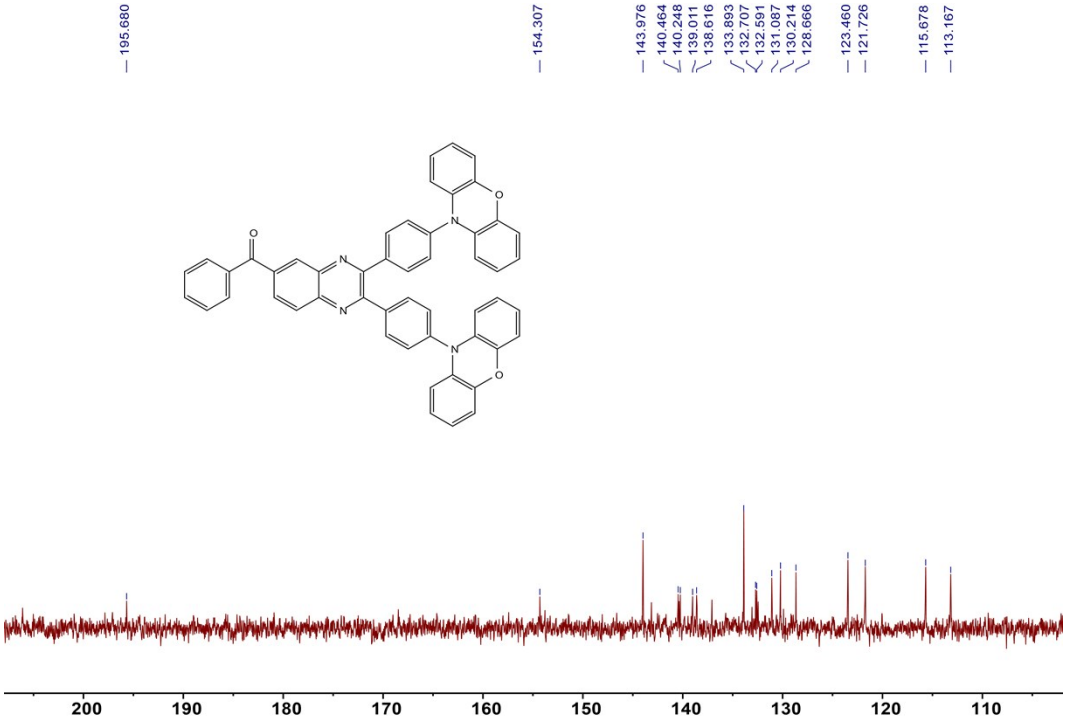

Fig. S15 $^{13}C$ NMR spectrum of **DPXZ-PQM** in $CDCl_3$.

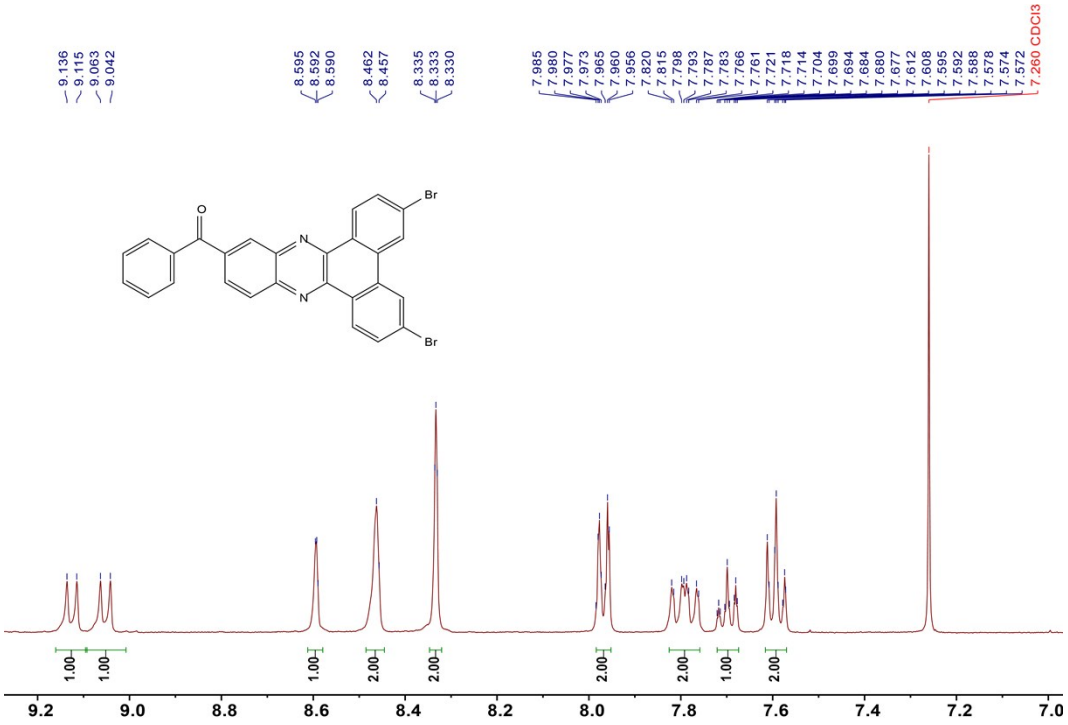


Fig. S16 $^{1}H$ NMR spectrum of **DBr-DPPM** in $CDCl_3$.

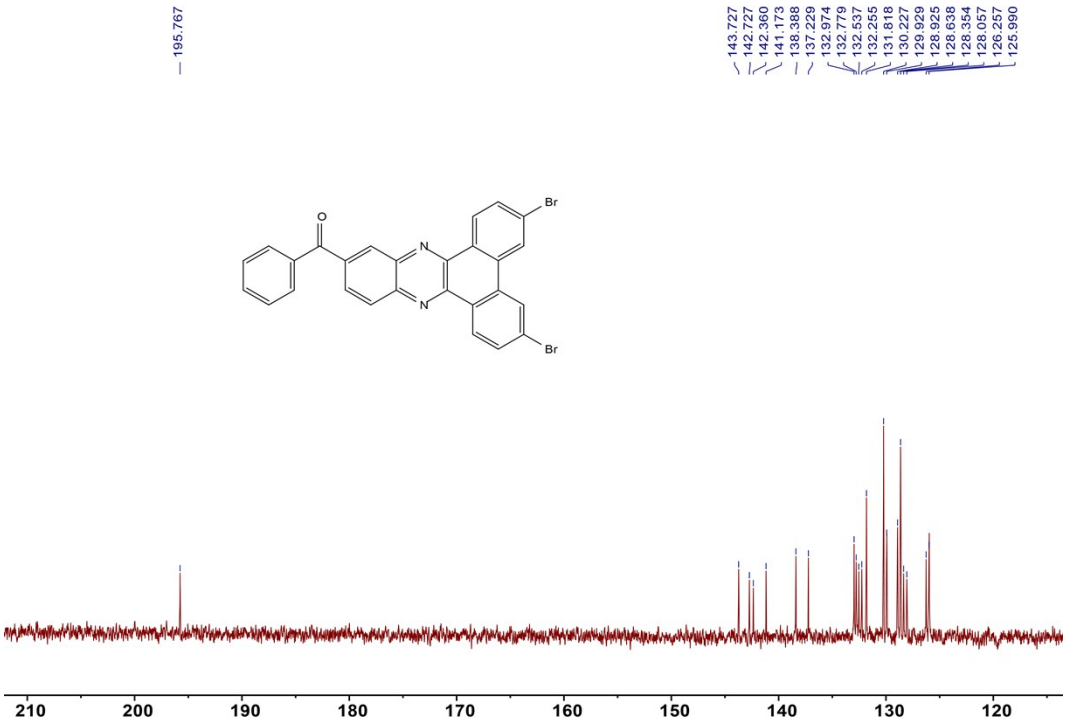

Fig. S17 $^{13}C$ NMR spectrum of **DBr-DPPM** in $CDCl_3$.

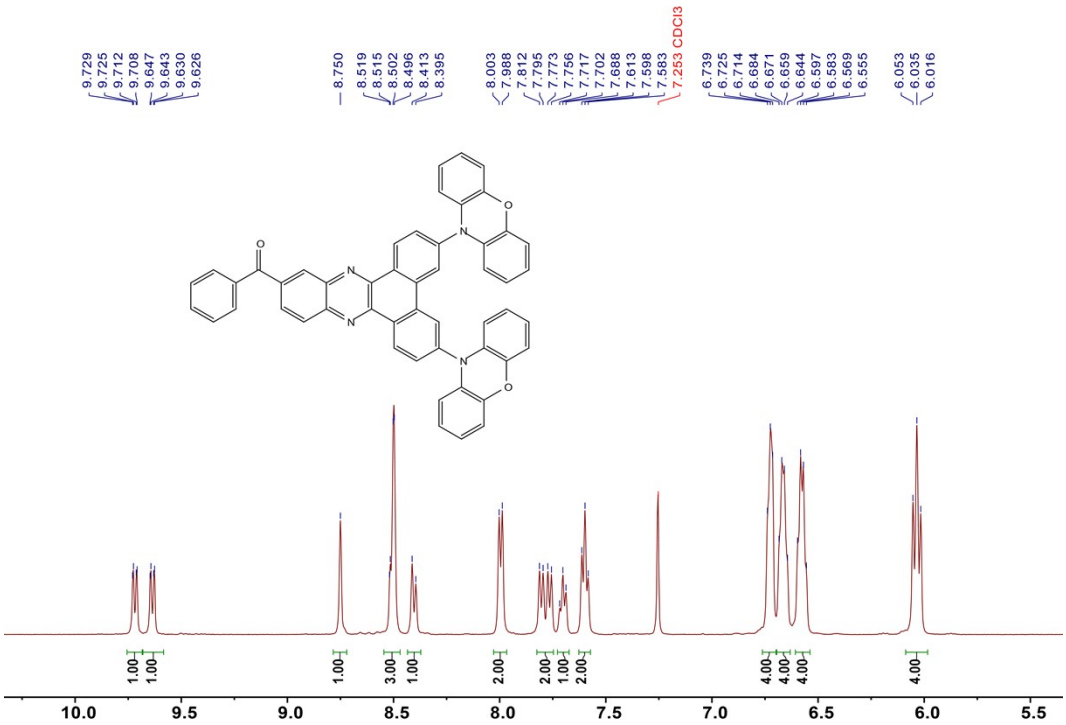


Fig. S18 $^{1}H$ NMR spectrum of **DPXZ-DPPM** in $CDCl_3$.

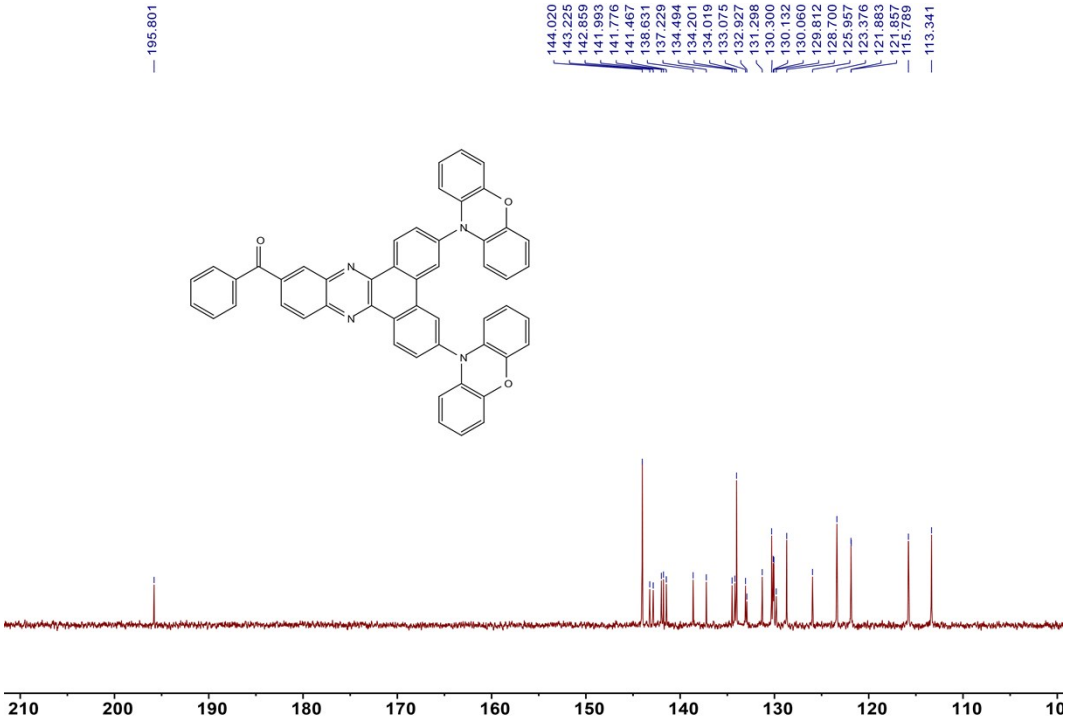

**Fig. S19** $^{13}C$ NMR spectrum of **DPXZ-DPPM** in $CDCl_3$.

## 9. References

[S1] Runge E.; Gross, E. K. U. Density-Functional Theory for Time-Dependent Systems. *Phys. Rev. Lett.*, 1984, **52**, 997.

[S2] Wang, S.; Cheng, Z.; Song, X.; Yan, X.; Ye, K.; Liu, Y.; Yang, G.; Wang Y. Highly Efficient Long-Wavelength Thermally Activated Delayed Fluorescence OLEDs Based on Dicyanopyrazino Phenanthrene Derivatives. *ACS Appl. Mater. Interfaces*, 2017, **9**, 9892−9901.

[S3] Frisch, M. J.; Trucks, G. W.; Schlegel, H. B.; Scuseria, G. E.; Robb, M. A.; Cheeseman, J. R.; Scalmani, G.; Barone, V.; Petersson, G. A.; Nakatsuji, H.; et al. *Gaussian Inc 16*, revision A.03; Gaussian Inc.: Wallingford, CT, 2016.

[S4] Yang, T.; Liang, B.; Cheng, Z.; Li, C.; Lu, G.; Wang Y. Construction of Efficient Deep-Red/Near-Infrared Emitter Based on a Large π-Conjugated Acceptor and Delayed Fluorescence OLEDs with External Quantum Efficiency of over 20%. *J. Phys. Chem. C*, 2019, **123**, 18585-18592.